Journal of Applied Polymer Science

Needleless Emulsion Electrospinning for Scalable Fabrication of Core–Shell Nanofibers

Zhengping Zhou,[1] Xiang-Fa Wu,[1] Yichun Ding,[1] Meng Yu,[1] Youhao Zhao,[1] Long Jiang,[1] Chengluan Xuan,[2] Chengwen Sun[2]

[1]Department of Mechanical Engineering, North Dakota State University, Fargo, North Dakota 58108-6050
[2]Department of Pharmaceutical Sciences, North Dakota State University, Fargo, North Dakota 58108-6050
Correspondence to: X.-F. Wu (E-mail: xiangfa.wu@ndsu.edu)

ABSTRACT: This article reports a new needleless emulsion electrospinning method for scale-up fabrication of ultrathin core–shell polyacrylonitrile (PAN)/isophorone diisocyanate (IPDI) fibers. These core–shell fibers can be incorporated at the interfaces of polymer composites for interfacial toughening and self-repairing due to polymerization of IPDI triggered by environmental moisture. The electrospinnable PAN/IPDI emulsion was prepared by blending PAN/*N*,*N*-dimethylformamide and IPDI/*N*,*N*-dimethylformamide solutions (with the solute mass fraction of 1 : 1). The electrospinning setup consisted of a pair of aligned metal wires as spinneret (positive electrode) to infuse the PAN/IPDI emulsion and a rotary metal disk as fiber collector (negative electrode). The formed ultrathin core–shell PAN/IPDI fibers were collected with the diameter in the range from 300 nm to 3 μm depending on the solution concentration and process parameters. Optical microscopy, scanning electron microscopy, and Fourier transform infrared spectroscopy were used to characterize the core–shell nanostructures. Dependencies of the fiber diameter on the PAN/IPDI concentration, wire spacing, and wire diameter were examined. Results show that needleless emulsion electrospinning provides a feasible low-cost manufacturing technique for scalable, continuous fabrication of core–shell nanofibers for potential applications in self-repairing composites, drug delivery, etc. © 2014 Wiley Periodicals, Inc. J. Appl. Polym. Sci. **2014**, *131*, 40896.

KEYWORDS: core–shell nanofibers; isophorone diisocyanate; needleless electrospinning; polyacrylonitrile

Received 16 December 2013; accepted 18 April 2014
DOI: 10.1002/app.40896

INTRODUCTION

Continuous nanofibers of natural and synthetic polymers, carbon, metals, metal oxides, etc. fabricated by means of the low-cost top-down electrospinning technique and related post-processing represent a new class of one-dimensional (1D) nanostructured materials.[1–9] Rapidly expanding applications of these advanced nanofibers have been identified in recent years, including protective clothing and wound dressing,[10–12] fine filtration,[13–15] nanofiber-reinforced polymer matrix composites (PMCs),[16–22] scaffolds for tissue growth,[23–28] drug delivery,[29–31] and energy harvesting, conversion and storage,[32–38] among others. The classic electrospinning technique has also been extended to produce core–shell and hollow nanofibers by replacing the single needle (nozzle) with a coaxial spinneret, i.e., coelectrospinning,[39–43] in which two polymer solutions are infused into the interior and exterior nozzles to form the core and shell materials, respectively. In addition, coelectrospun core–shell nanofibers can be further converted into hollow nanofibers via extracting or thermal decomposition of the core material.[40] Continuous core–shell and hollow nanofibers can be potentially used for gas and liquid transport, drug delivery, electrode materials of supercapacitors and rechargeable batteries, encapsulation of healing agent for self-repairing composites,[22,42,44] etc. In addition, core–shell nanofibers can also be produced by means of single-needle-based emulsion electrospinning.[45–47] During this process, the core and shell materials are first dissolved separately into proper solvents to form two immiscible or less-miscible solutions. Proper mixture of the two solutions leads to an electrospinnable emulsion. Upon electrospinning of the emulsion, droplets of one solution are encapsulated into the second solution of the electrospinning jet, deformed, and elongated, and consequently form the core of the core–shell fiber. In principle, emulsion electrospinning can be utilized for producing a variety of core–shell and hollow nanofibers based on the conventional electrospinning setup with a single spinneret (nozzle), although appropriate preparation of an electrospinnable emulsion is required.

Yet, the productivity of single-needle-based coelectrospinning and emulsion electrospinning is very low, largely a few grams per day, which could not satisfy the demand of any practical

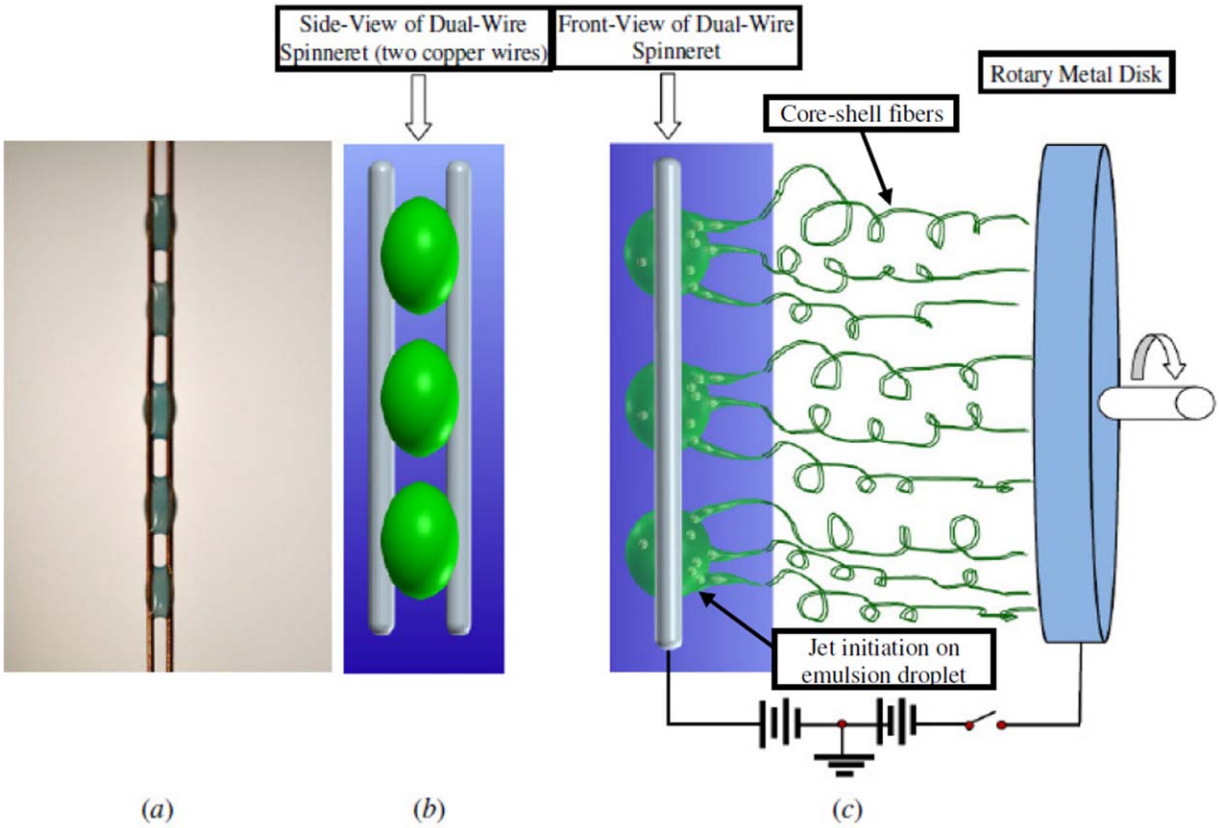

Figure 1. (a) Droplets of 10 wt % PAN/IPDI/DMF emulsion wetting on two closely aligned copper wires (the diameter of the copper wires: 0.78 mm; the volume of the emulsion droplet: ~0.1 mL; a small quantity of dye was dissolved for better visualization). (b) Side view and (c) front view of schematic setup of dual-wire emulsion electrospinning for scale-up fabrication of ultrathin core–shell fibers. During dual-wire emulsion electrospinning, droplets of the second polymer solution are enwrapped within the master droplets of the first polymer solution; multiple jets ejaculate from the master droplet due to electrohydrodynamic destabilization; enwrapped droplets within the jets are stretched and thinned under electrostatic force and eventually form the core material after drying. [Color figure can be viewed in the online issue, which is available at wileyonlinelibrary.com.]

biomedical and industrial applications. To date, substantial research effort has been devoted to enhancing the manufacturing productivity of core–shell nanofibers, such as utilizing destabilization of two thin immiscible polymer solution layers based on the principle of needleless electrospinning,[48–54] i.e., free-surface electrohydrodynamic jetting. However, such an approach may encounter technical difficulties because initiation of multiple jets from a thin dielectric liquid layer depends upon its electrohydrodynamic destabilization in electrostatic field. The wavelength of such an electrohydrodynamic destabilization highly relies on the surface (interface) tension, dielectric constant, mass density, and thickness of a thin liquid layer.[49,50] Nevertheless, it is challenging to simultaneously tune the parameters of two liquid layers (e.g., thickness) such that destabilizations of two immiscible liquid layers take place with very close wavelengths, which could guarantee the generation of stable core–shell jets. Initiation of jets due to destabilization of either the top or bottom liquid layer can be expected; however, in such a case, destabilization of the second liquid layer could be suppressed due to the different destabilization conditions. Therefore, new techniques for scale-up fabrication of ultrathin core–shell fibers are still desired in order to satisfy the ever-growing demand of core–shell fibers for broad applications in biomedical, industrial, and other sectors.

In this experimental study, a novel dual-wire emulsion electrospinning method was formulated for scale-up fabrication of ultrathin core–shell fibers. In the process, an emulsion made up with isophorone diisocyanate (IPDI)/*N*,*N*-dimethylformamide (DMF) solution droplets merged in a polyacrylonitrile (PAN)/DMF solution was delivered via a thin channel formed between two closely aligned wires as spinneret [coined as dual-wire spinneret as shown in Figure 1(a)].[55–58] After destabilization of the emulsion thread in the thin channel due to the electrocapillary force, the emulsion thread may form a chain of droplets sitting between the wires. The complex morphology of the droplets in the channel can facilitate the surface jetting, and the intrinsic electrocapillary force can further drive the emulsion to fill the channel between the wires as a capillary pump. To demonstrate this technique, in this study we prepared the electrospinnable emulsions via blending PAN/DMF and IPDI/DMF solutions with the mass fraction 1 : 1. Mass concentrations of 6%, 8%, 10%, 12%, and 16% were selected respectively for both PAN/DMF and IPDI/DMF solutions. The core–shell nanostructure of

the electrospun core–shell PAN/IPDI fibers was characterized by means of optical microscopy, scanning electron microscopy (SEM), and Fourier transform infrared (FTIR) spectroscopy. Dependencies of the fiber diameter and layered structures of the core–shell PAN/IPDI fibers on the spacing and diameter of the metal wires and the solution concentration were examined, respectively. Discussion on the experimental results and their governing mechanisms were made, and conclusion of the research was drawn.

EXPERIMENTAL

Experimental Setup

Figure 1(b,c) illustrates the setup of dual-wire emulsion electrospinning, which consists of a dual-wire spinneret (two closely aligned copper wires), a rotary aluminum disk (diameter: 25 cm and thickness: 2.5 mm) as the fiber collector, and two high-voltage direct-current (DC) power supplies (Gamma High Voltage Research, Inc., Ormond Beach, FL) carrying the positive and negative voltage outputs, respectively. Use of a DC power supply with a negative voltage output as illustrated in Figure 1(c) is to ensure that the electrical potential of the fiber collector is always below that of grounded surrounding parts such as the equipment and lab utilities, which can avoid nanofibers flying off the fiber collector during electrospinning process.

As illustrated in Figure 1(a,b), the two closely positioned straight wires (copper wires) form a capillary microchannel (dual-wire spinneret) that can be utilized to manipulate and deliver a small quantity of liquid via capillary effect or mechanical motion through an emulsion reservoir.[55–58] Droplets sitting between the wires can form either barrel-shaped droplets, which completely enwrap the two wires, or droplet-bridges, which partially wet the two wires, depending upon the wetting behavior of the system.[57,58] Superior to droplets sitting on a single wire, when the wire spacing is small, the microchannel between the two thin wires can generate sufficient capillary force to pump the droplets to move along the wires in the form of droplet-bridge, i.e., wetting the wires or wicking. Recent experimental study[56] indicated that the wicking kinetics of droplet spreading on a dual-wire spinneret roughly obeyed the simple Lucas–Washburn law,[59,60] i.e., given a wire spacing, the meniscus displacement is proportional to the complete wicking time (i.e., the time interval from the start of droplet spreading to its disappearance). When applying a high DC voltage between the dual-wire spinneret and the fiber collector, the electrostatic force acting on the liquid can destabilize the liquid-bridge and form multiple droplets as illustrated in Figure 1(b); each droplet may initiate one or multiple jets as illustrated in Figure 1(c) due to the complex morphology of the droplets. When the two ends of the dual-wire spinneret are connected to an emulsion reservoir or a digitally controlled syringe pump, the capillary force can drive the emulsion to the jetting zone [Figure 1(c)]. This pumping process can also be realized via oscillating the dual-wire spinneret through the emulsion reservoir (mechanical translation). Thus, scalable continuous emulsion electrospinning can be sustained using the present setup. In addition, use of dual-wire spinneret can significantly suppress fast evaporation of volatile solvent via reducing exposure of the emulsion to open air.

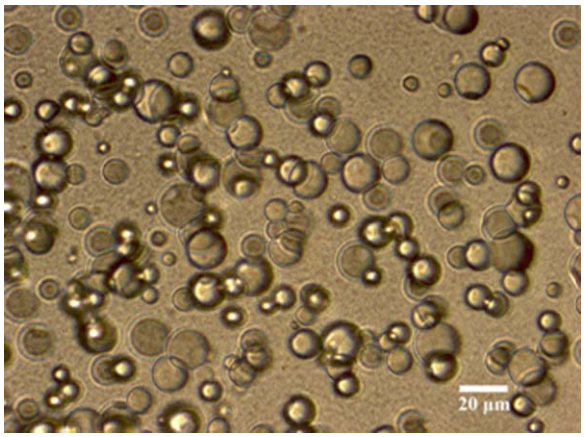

Figure 2. Optical micrograph of an IPDI/PAN/DMF emulsion. The emulsion was prepared via blending 10 wt % PAN/DMF solution with 10 wt % IPDI/DMF solution and placed in laboratory at room temperature without disturbance for 2 days. [Color figure can be viewed in the online issue, which is available at wileyonlinelibrary.com.]

Materials and Emulsion Preparation and Characterization

PAN powder ($M_w = 150{,}000$), liquid IPDI, and DMF anhydrous (99.8%) were purchased from Sigma-Aldrich (St. Louis, MO) without further purification. To form the emulsions, two precursor solutions, i.e., the PAN/DMF solutions with the mass concentration of 6%, 8%, 10%, 12%, and 14% PAN and IPDI/DMF solutions with the equal mass concentrations of IPDI, were first prepared separately via dissolving the PAN powder and liquid IPDI in DMF, respectively. Each pair of as-prepared PAN/DMF and IPDI/DMF solutions with the equal mass concentration was continuously stirred on a hot-plate at 75°C for 4 h, and then blended together at the mass fraction 1 : 1. The resulting ternary PAN/IPDI/DMF mixture was stirred on the hot-plate at 75°C for another 4 h and then stirred slowly at room temperature till the electrospinning test. Furthermore, the transient shear viscosity of the PAN/IPDI/DMF solutions was measured using a TA ARG2 Rheometer (TA Instruments, New Castle, DE) within the range of shear rate from 0 to 1000 s^{-1} at room temperature.

In addition, morphologies of as-prepared emulsions were characterized using an optical microscope (IX 71 Olympus with the objective magnification of ×40) as shown in Figure 2, from which it can be observed that well-formed droplets (IPDI/DMF solution) dispersed uniformly in PAN/DMF solution.

Needleless Emulsion Electrospinning for Scale-Up Fabrication of Core–Shell PAN/IPDI Nanofibers

As illustrated in Figure 1(c), during the electrospinning process, the rotary disk was placed over the dual-wire plane with a vertical distance ~25 cm and powered by a DC electrical motor with adjustable angular velocity. For the purpose of comparative study, in the case of the PAN/DMF and IPDI/DMF solutions with the mass concentration of 10%, the copper wires with two different diameters (0.28 and 0.78 mm) and two different values of spacing (0 and 0.30 mm) were chosen for the dual-wire spinneret. In addition, to investigate the effect of mass concentration of the PAN/IPDI/DMF solution on the diameter of core–

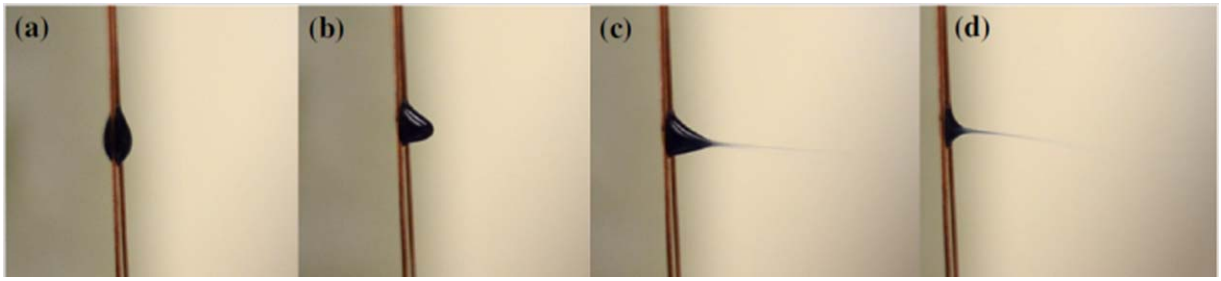

Figure 3. Snapshots of dual-wire emulsion electrospinning process with gradually increasing DC voltage of the wires (a) 0 kV; (b) ~10 kV; and (c, d) ~15 kV. (The diameter of the copper wires: 0.78 mm; the volume of the droplet: ~0.1 mL; the distance between the dual-wire spinneret and the fiber collector: 20 cm; the emulsion was prepared via blending 10 wt % PAN/DMF solution with 10 wt % IPDI/DMF solution; a small quantity of dye was dissolved in the solution for better visualization). [Color figure can be viewed in the online issue, which is available at wileyonlinelibrary.com.]

shell PAN/IPDI fibers, PAN/IPDI/DMF emulsions with five mass concentrations were used for the needleless emulation electrospinning test (i.e., 6%, 8%, 10%, 12%, and 14%). In each electrospinning test, the diameter and spacing of the two copper wires were fixed as 0.28 and 0.30 mm, respectively.

In the present study, the dual-wire emulsion electrospinning test was performed at room temperature. Prior to the test, the two copper wires of the spinneret were wiped with acetone to clean and maintain constant surface energy. Given a set of parameters (i.e., the wire diameter and spacing) of the dual-wire spinneret, the emulsion was first delivered to the spinneret manually to form multiple droplet-bridges [see Figure 1(a)]. Once the spinneret potential was increased up to +25 kV and the fiber collector potential was decreased down to −20 kV, jets started to initiate from the droplet bridges as illustrated in Figure 1(c). Figure 3 shows the snapshots of a typical jetting process of an emulsion droplet sitting on the dual-wire spinneret, where the DC voltage between the dual-wire spinneret and fiber collector was gradually increased. The electrospinning process can be maintained with continuous supply of emulsion via electrocapillary pumping or mechanical translation of the emulsion. The morphology of the electrospinnable emulsion and the core–shell structure of the resulting ultrathin PAN/IPDI fibers were characterized by means of optical microscopy (IX 71 Olympus with the objective magnification of ×40), SEM (JEOL JSM-7600F), and FTIR characterizations.

RESULTS AND DISCUSSIONS

The optical micrographs as shown in Figure 4 are the typical ultrathin core–shell PAN/IPDI fibers produced by using the present emulsion electrospinning method based on the PAN/IPDI/DMF emulsion with the PAN/IPDI mass concentration 10 wt % at varying process parameters as follows. To produce the PAN/IPDI fibers as shown in Figure 4(a,b), the dual-wire spinneret consisted of two identical copper wires of the diameter 0.28 mm and wire spacing 0.30 mm. It can be observed from Figure 4(a,b) that the core–shell nanostructures were well formed with uniform morphologies of the interior liquid IPDI core and exterior solid PAN shell.

To examine the effect of wire spacing on the morphology of the core–shell PAN/IPDI fibers, a dual-wire spinneret with zero spacing was further utilized, whereas the rest process parameters were unaltered. Figure 4(c) shows the typical optical micrograph of the resulting core–shell PAN/IPDI fibers. It can be observed that though the core–shell PAN/IPDI fibers were well formed with smooth morphologies of the interior core and exterior shell, the diameter of the core–shell fibers showed a large variation. Multiple measurements showed that the average diameter of the IPDI core is ~0.7 μm, whereas the average exterior diameter of the PAN shell is ~1.9 μm, which are much larger than those with the wire spacing of 0.30 mm. In this case, relatively large droplets can assume on the dual-wire spinneret, which ultimately developed into Taylor cones with a large size, corresponding to the large diameter of the final core–shell nanofibers though detailed electrohydrodynamic mechanisms are still not available yet.

To take into account the effect of the wire diameter on the diameter and morphology of the final core–shell PAN/IPDI fibers, a dual-wire spinneret with the wire diameter 0.78 mm and wire spacing 0.30 mm was used, and the rest process parameters were still maintained the same. Figure 4(d) shows the typical optical micrograph of the resulting core–shell PAN/IPDI fibers. From Figure 4(d), it can be found that the core–shell PAN/IPDI fibers still carried well-formed morphologies of the interior core and exterior shell. However, the diameter of the core–shell fibers had a much larger variation than those in the two cases investigated above. In this case, the average diameters of the IPDI core and PAN shell are ~0.8 and ~2.0 μm, respectively, slightly larger than those based on the dual-wire spinneret with zero spacing. In this case, after electrohydrodynamic destabilization, droplets with a larger size assumed on the dual-wire spinneret, which finally resulted in the core–shell PAN/IPDI nanofibers with larger diameters. As a result, the wire diameter and spacing of the dual-wire spinneret combined with other process and material parameters can be used for tuning the geometries of electrospun core–shell fibers.

The structure of the present core–shell PAN/IPDI nanofibers was also examined by means of SEM. During the process, as-prepared core–shell PAN/IPDI nanofibers made from 10 wt % PAN/IPDI/DMF emulsion were consolidated into an epoxy resin. After curing in room temperature, five pieces of sample slides were prepared using a sharp razor, coated with carbon, and SEM-scanned. Figure 5(a) shows the cross-section of a

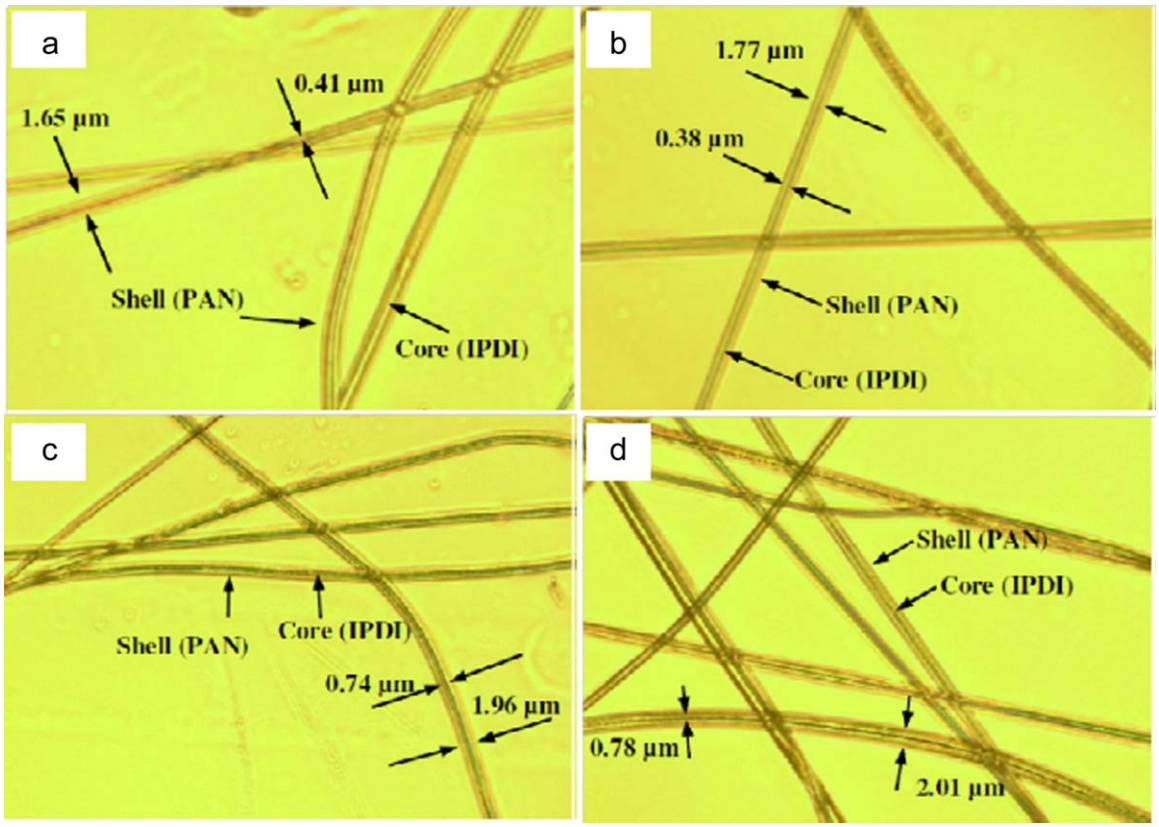

Figure 4. Optical micrograph of emulsion-electrospun core–shell PAN/IPDI fibers based on a dual-wire spinneret: (a, b) The diameter of copper wires was 0.28 mm and wire spacing was 0.30 mm; (c) the diameter of copper wires was 0.28 mm and there was free wire spacing; (d) the diameter of copper wires was 0.78 mm and wire spacing was 0.30 mm. [Color figure can be viewed in the online issue, which is available at wileyonlinelibrary.com.]

scissored core–shell PAN/IPDI nanofiber embedded in epoxy resin, where the core–shell structure can be clearly detected, and the liquid IPDI dissipated due to polymerization triggered by the air. Figure 5(b) shows the side view of a cracked core–shell PAN/IPDI nanofiber, from which the cracked shell material can be obviously observed and the liquid IPDI solidified into porous structure after polymerization.

In addition, FTIR was further used to validate the chemical composition of the resulting PAN/IPDI nanofibers. Figure 6 shows the comparative FTIR spectra of the pure PAN nanofibers

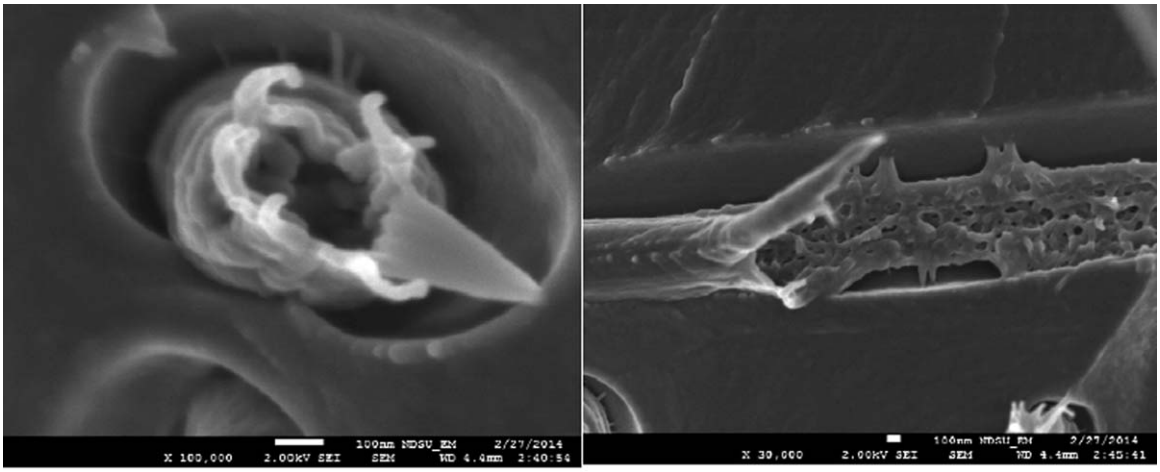

Figure 5. SEM micrographs of (a) cross-section of a scissored core–shell PAN/IPDI nanofiber and (b) side view of a cracked core–shell PAN/IPDI embedded in epoxy resin.

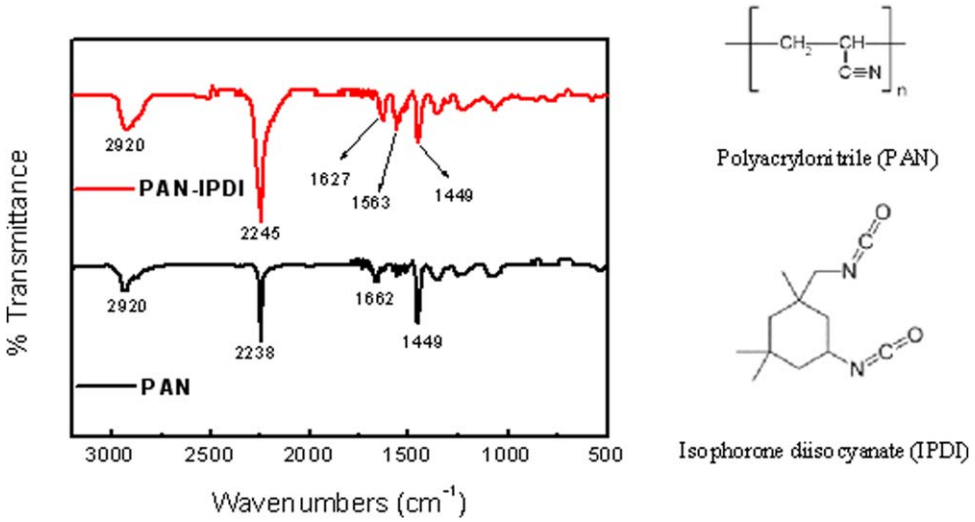

Figure 6. FTIR spectra of both pure PAN nanofibers and typical emulsion-electrospun core–shell PAN/IPDI nanofibers. [Color figure can be viewed in the online issue, which is available at wileyonlinelibrary.com.]

produced by single-needle-based electrospinning and the present core–shell PAN/IPDI fibers. The FTIR results confirm the existence of IPDI in the core–shell fibers. In the spectra of PAN nanofibers, the characteristic absorption bands at 2920, 2238, 1662, and 1449 cm^{-1} are, respectively, assigned to νC—H stretching, νC≡N stretching, δC—H bond bending, and δCH_2 asymmetric vibration.[61] In contrast, in the spectra of PAN/IPDI fibers, two obvious peaks at ~2245 and ~2920 cm^{-1} exist due to the isocyanate νN═C═O and νC—H stretching vibrations in IPDI, respectively.[62] Besides, bands at 1627 and 1563 cm^{-1} due to C═O vibration in the —NCO group are in good agreement with the existence of IPDI in the PAN/IPDI core–shell nanofibers. These characteristic infrared spectra combined with the layered structure observed by optical microscopy above confirm the core–shell structure of the obtained PAN/IPDI fibers.

To examine the effect of PAN/IPDI mass concentration on the diameter of the resulting core–shell nanofibers, five PAN/IPDI/DMF emulsions with the PAN/IPDI mass concentration of 6%, 8%, 10%, 12%, and 14% (mass fraction PAN : IPDI = 1 : 1) were prepared and tested as aforementioned. Figure 7 shows the transient viscosity of the five emulsions tested on a TA ARG2 Rheometer (TA Instruments, New Castle, DE). It can be found from Figure 7 that given a shear rate, the transient viscosity increases with increasing mass concentration. Furthermore, in the case of the PAN/IPDI mass concentration of 6% and 8%, the viscosity of the PAN/IPDI/DMF emulsion appears nearly constant in the range of testing shear rate from 0 to 1000 s^{-1}. However, in the case of PAN/IPDI mass concentration of 10%, 12%, and 14%, the viscosity decreases noticeably at the high shear rate. Such shear-thinning effect is typically observed in polymer solutions at high shear rates due to delayed chain relaxation.[63,64] The variation of the exterior diameter of the core–shell PAN/IPDI with varying PAN/IPDI mass concentration is tabulated in Table I and shown in Figure 8(f). It can be found that the average fiber diameter increases rapidly with increasing PAN/IPDI concentration from 144 nm at 6 wt % to 3426 nm at 14 wt %. Correspondingly, the deviation of the fiber diameter also increases rapidly with increasing PAN/IPDI concentration. These average and deviation values of fiber diameter were obtained by performing ~100 measurements from ~20 to 30 SEM micrographs of the typical core–shell PAN/IPDI fibers. Figure 8(a–e) shows the SEM micrographs of typical PAN/IPDI nanofibers produced at varying PAN/IPDI mass concentrations. It can be detected that the diameter variation of these ultrathin PAN/IPDI fibers becomes larger and larger with increasing PAN/IPDI mass concentration. Thus, it can be concluded that to produce core–shell fibers with uniform diameter, relatively low mass concentration is preferred in needleless emulsion electrospinning.

It is worthy to point out that these ultrathin core–shell PAN/IPDI fibers are technologically important to self-repairing PMCs.[22,42,44] The core–shell PAN/IPDI fibers can be embedded at the interfaces of fiber-reinforced PMCs via depositing them

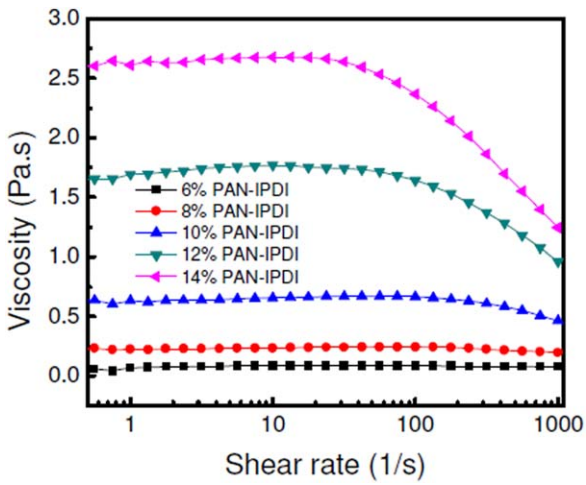

Figure 7. Variation of the shear viscosity with varying shear rate for PAN/IPDI (mass ratio = 1 : 1)/DMF solutions at varying PAN/IPDI mass concentrations of 6%, 8%, 10%, 12%, and 14%. [Color figure can be viewed in the online issue, which is available at wileyonlinelibrary.com.]

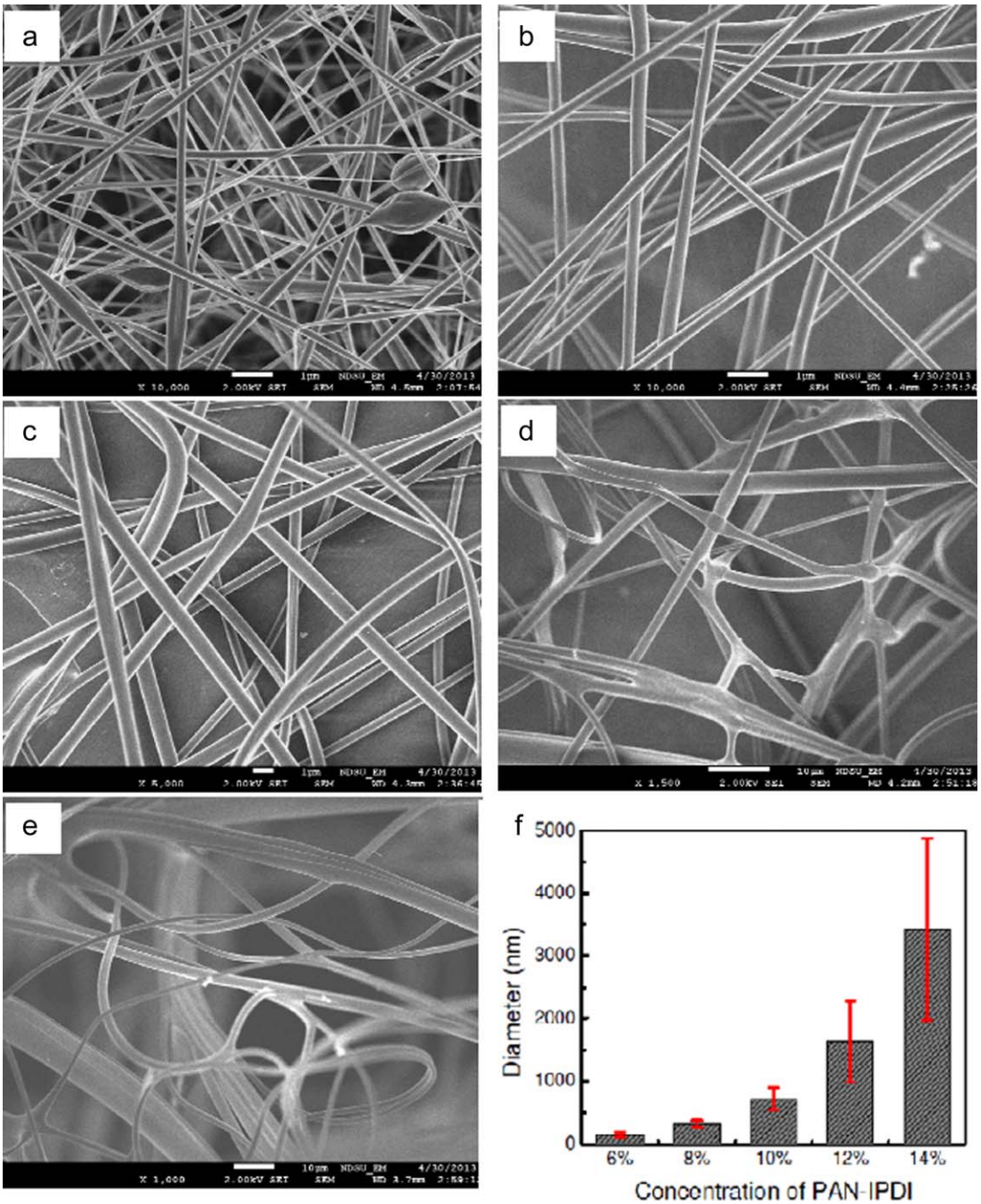

Figure 8. SEM micrographs of typical emulsion-electrospun core–shell PAN/IPDI fibers with varying mass concentration of PAN/IPDI: (a) 6%, (b) 8%, (c) 10%, (d) 12%, and (e) 14% by weight concentration in DMF (copper wire diameter: 0.28 mm and wire spacing: 0.30 mm); (f) Variation of the exterior diameter of emulsion-electrospun core–shell PAN/IPDI fibers with varying mass concentration of PAN and IPDI (copper wire diameter: 0.28 mm and wire spacing: 0.30 mm). [Color figure can be viewed in the online issue, which is available at wileyonlinelibrary.com.]

Table I. Average Exterior Diameters of the PAN/IPDI Nanofibres Produced by Means of Needleless Emulsion Electrospinning at Varying Solution Mass Concentrations

	Solution concentration (wt %) (PAN : IPDI = 1 : 1 by weight)				
	6	8	10	12	14
Exterior diameter of nanofiber (nm)	144 ± 50	314 ± 55	710 ± 180	1630 ± 640	3430 ± 1450

onto the prepreg sheets before thermal press molding or onto the fiber fabrics before resin infusion. After curing, the core–shell PAN/IPDI nanofibers will form ultrathin self-repairing interlayers with rich PAN/IPDI nanofibers. Upon occurrence of interfacial damage such as delamination that scissors the PAN/IPDI nanofibers, the liquid healing-agent IPDI will autonomically release at the locus of damage under the action of capillary forces and local stresses and polymerize upon catalysis with the aid of local and environmental water or moisture.[22,42,44]

Moreover, the present experimental study also opens an innovative route in electrospinning and nanomanufacturing for scale-up continuous fabrication of core–shell nanofibers because multiple core–shell jets can form simultaneously from the dual-wire spinneret. Also, the experimental observations available in this study can provide valuable first-hand experimental data to advance understanding and exploitation of the fundamental electrohydrodynamic theories for intelligent mass production of core–shell nanofibers.

CONCLUSIONS

In summary, a novel dual-wire emulsion electrospinning method has been developed and demonstrated for successful scalable continuous fabrication of core–shell nanofibers. Effects of several process and material parameters on the fiber diameter have been examined. The experimental results indicated that the average fiber diameter increases with increasing either wire diameter or mass concentration, or decreasing wire spacing of the dual-wire spinneret. The present experimental study also provides useful first-hand data to explore the fundamental understanding of modern electrospinning processes. The needleless dual-wire emulsion electrospinning technique can be exploited for low-cost mass production of core–shell nanofibers for large-scale applications in broad areas.

ACKNOWLEDGMENTS

The financial support of the research work by National Science Foundation (award no.: CMMI-1234297), ND NASA EPSCoR (NASA Grant #NNX07AK91A and seed grant: 43500-2490-FAR18640), NDSU Development Foundation (FAR17475), and ND Soybean Council (FAR19227) was gratefully acknowledged. Z. Zhou gratefully appreciated the ND EPSCoR Doctoral Dissertation Fellowship Award (2013–2014).

REFERENCES

1. Reneker, D. H.; Chun, I. *Nanotechnology* **1996**, *7*, 216.
2. Doshi, J.; Reneker, D. H. *J. Electrostatics* **1995**, *35*, 151.
3. Huang, Z. M.; Zhang, Y. Z.; Kotaki, M.; Ramakrishna, S. *Compos. Sci. Technol.* **2003**, *63*, 2223.
4. Dzenis, Y. *Science* **2004**, *304*, 1917.
5. Li, D.; Xia, Y. N. *Adv. Mater.* **2004**, *16*, 1151.
6. Reneker, D. H.; Yarin, A. L.; Zussman, E.; Xu, H. *Adv. Appl. Mech.* **2007**, *41*, 43.
7. Greiner, A.; Wendorff, J. H. *Angew. Chem. Int. Ed.* **2007**, *46*, 5670.
8. Ramaseshan, R.; Sundarragan, S.; Jose, R.; Ramakrishna, S. *J. Appl. Phys.* **2007**, *102*, 111101.
9. Reneker, D. H.; Yarin, A. L. *Polymer* **2008**, *49*, 2387.
10. Gibson, P.; Schreuder-Gibson, H.; Rivin, D. *Colloid Surf. A Physicochem. Eng. Asp.* **2001**, *187*, 469.
11. Smith, D.; Reneker, D. H.; Kataphinan, W.; Dabney, A. U. S. *Pat.* 6,821,479 (**2001**).
12. Smith, D.; Reneker, D. H. U. S. Pat. 6,753,454 (**2004**).
13. Gopal, R.; Kaur, S.; Ma, Z. W.; Chan, C.; Ramakrishna, S.; Matsuura, T. *J. Membr. Sci.* **2006**, *281*, 581.
14. Maze, B.; Tafreshi, H. V.; Wang, Q.; Pourdeyhimi, B. *Aerosol Sci.* **2007**, *38*, 550.
15. Barhate, R. S.; Ramakrishna, S. *J. Membr. Sci.* **2007**, *296*, 1.
16. Dzenis, Y. *Science* **2008**, *319*, 419.
17. Chen, F.; Peng, X. W.; Li, T. T.; Chen, S. L.; Wu, X. F.; Reneker, D. H.; Hou, H. Q. *J. Phys. D Appl. Phys.* **2008**, *41*, 025308.
18. Cheng, C. Y.; Chen, J.; Chen, F.; Wu, X. F.; Reneker, D. H.; Hou, H. Q. *J. Appl. Polym. Sci.* **2010**, *116*, 1581.
19. Chen, Q.; Zhang, L. F.; Rahman, A.; Zhou, Z. P.; Wu, X. F.; Fong, H. *Compos. A: Appl. Sci. Manuf.* **2011**, *42*, 2036.
20. Chen, Q.; Zhang, L. F.; Zhao, Y.; Wu, X. F.; Fong, H. *Compos. B: Eng.* **2012**, *43*, 309.
21. Chen, Q.; Zhang, L. F.; Yoon, M. K.; Wu, X. F.; Arefin, R. H.; Fong, H. *J. Appl. Polym. Sci.* **2012**, *124*, 444.
22. Wu, X. F.; Rahman, A.; Zhou, Z. P.; Pelot, D. D.; Sinha-Ray, S.; Chen, B.; Payne, S.; Yarin, A. L. *J. Appl. Polym. Sci.* **2013**, *129*, 1383.
23. Li, W. J.; Laurencin, C. T.; Caterson, E. J.; Tuan, R. S.; Ko, F. K. *J. Biomed. Mater. Res.* **2002**, *60*, 613.
24. Matthews, J. A.; Wnek, G. E.; Simpson, D. G.; Bowlin, G. L. *Biomacromolecules* **2002**, *3*, 232.
25. Burger, C.; Hsiao, B. S.; Chu, B. *Ann. Rev. Mater. Res.* **2006**, *36*, 333.
26. Pham, Q. P.; Sharma, U.; Mikos, A. G. *Tissue Eng.* **2006**, *12*, 1197.
27. Barnes, C. P.; Sell, S. A.; Boland, E. D.; Simpson, D. G.; Bowlin, G. L. *Adv. Drug Deliv. Rev.* **2007**, *59*, 1413.
28. Xie, J.; Li, X.; Xia, Y. *Nat. Mater.* **2008**, *29*, 1775.
29. Kenawy, E. R.; Bowlin, G. L.; Mansfield, K.; Layman, J.; Simpson, D. G.; Sanders, E. H.; Wnek, G. E. *J. Control. Release* **2002**, *81*, 57.
30. Chew, S. Y.; Wen, Y.; Dzenis, Y.; Leong, K. W. *Curr. Pharm. Design* **2006**, *12*, 4751.
31. Liang, D. H.; Hsiao, B. S.; Chu, B. *Adv. Drug Deliv. Rev.* **2007**, *59*, 1392.
32. Kim, C.; Yang, K. S. *Appl. Phys. Lett.* **2003**, *83*, 1216.
33. Kim, C.; Ngoc, B. T. N.; Yang, K. S.; Kojima, M.; Kim, Y. A.; Kim, Y. J.; Endo, M.; Yang, S. C. *Adv. Mater.* **2007**, *19*, 2341.
34. Ji, L. W.; Zhang, X. W. *Carbon* **2009**, *47*, 3219.
35. Schulz, D. L.; Hoey, J.; Smith, J.; Elangovan, A.; Wu, X.; Akhatov, I.; Payne, S.; Moore, J.; Boudjouk, P.; Pederson, L.;

Xiao, J.; Zhang, J. *Electrochem. Solid State Lett.* **2010**, *13*, A143.

36. Zhang, X. W.; Ji, L. W.; Toprakci, O.; Liang, Y. Z.; Alcoutlabi, M. *Polym. Rev.* **2011**, *51*, 239.
37. Zhou, Z. P.; Wu, X. F.; Fong, H. *Appl. Phys. Lett.* **2012**, *100*, 023115.
38. Zhou, Z. P.; Wu, X. F. *J. Power Source* **2013**, *222*, 410.
39. Sun, Z. C.; Zussman, E.; Yarin, A. L.; Wendorff, J. H.; Greiner, A. *Adv. Mater.* **2003**, *15*, 1929.
40. Li, D.; Babel, A.; Jenekle, S. A.; Xia, Y. N. *Adv. Mater.* **2004**, *16*, 2062.
41. McCann, J. T.; Li, D.; Xia, Y. N. *J. Mater. Chem.* **2005**, *15*, 735.
42. Sinha-Ray, S.; Pelot, D. D.; Zhou, Z. P.; Rahman, A.; Wu, X. F.; Yarin, A. L. *J. Mater. Chem.* **2012**, *22*, 9138.
43. Moghe, A. K.; Gupta, B. S. *Polym. Rev.* **2008**, *48*, 353.
44. Wu, X. F.; Yarin, A. L. *J. Appl. Polym. Sci.* **2013**, *15*, 2225.
45. Bazilevsky, A. V.; Yarin, A. L.; Megaridis, C. M. *Langmuir* **2007**, *23*, 2311.
46. Xu, X. L.; Zhuang, X. L.; Chen, X. S.; Wang, X. R.; Yang, L. X.; Jing, X. B. *Macromol. Rapid Commun.* **2006**, *27*, 1637.
47. Yarin, A. L. *Polym. Adv. Tech.* **2011**, *22*, 310.
48. Yarin, A. L.; Zussman, E. *Polymer* **2004**, *45*, 2977.
49. Theron, A.; Yarin, A. L.; Zussman, E.; Kroll, E. *Polymer* **2005**, *46*, 2889.
50. Wu, X. F.; Dzenis, Y. A. *J. Phys. D* **2005**, *38*, 2848.
51. Lukas, D.; Sarkar, A.; Pokorny, P. *J. Appl. Phys.* **2008**, *103*, 084309.
52. Miloh, T.; Spivak, B.; Yarin, A. L. *J. Appl. Phys.* **2009**, *106*, 114910.
53. Lukas, D.; Sarkar, A.; Martinova, L.; Vodsedalkova, K.; Lubasova, D.; Chaloupek, J.; Pokorny, P.; Mikes, P.; Chvojka, J.; Komarek, M. *Textile Prog.* **2009**, *41*, 59.
54. Forward, K. M.; Flores, A.; Rutledge, G. C. *Chem. Eng. Sci.* **2013**, *104*, 250.
55. Princen, H. M. *J. Colloid Interface Sci.* **1970**, *34*, 171.
56. Guceri, S.; Gogoti, Y. G.; Kuznetsov, V., Eds. NATO Science Series II: Mathematics, Physics and Chemistry; Kluwer Academic Publishers, **2004**; Vol. 169, p. 175.
57. Wu, X. F.; Bedarkar, A.; Vaynberg, K. A. *J. Colloids Interface Sci.* **2010**, *341*, 326.
58. Bedarkar, A.; Wu, X. F.; Vaynberg, A. *Appl. Surface Sci.* **2010**, *256*, 7260.
59. Lucas, R. *Kollid Z.* **1918**, *23*, 15.
60. Washburn, E. W. *Phys. Rev.* **1921**, *17*, 273.
61. Moreno, M.; Ana, M. A. S; Gonzalez, G.; Benavente, E. *Electrochim. Acta* **2010**, *55*, 1323.
62. Zhou, S. J.; Ma, C. Y.; Meng, Y. Y.; Su, H. F.; Zhu, Z.; Deng, S. L.; Xie, S. Y. *Nanotechnology* **2012**, *23*, 055708.
63. Zhou, Z. P.; Wu, X. F.; Gao, X. Q.; Jiang, L.; Zhao, Y.; Fong, H. *J. Phys. D: Appl. Phys.* **2011**, *44*, 435401.
64. Barnes, H. A.; Roberts, G. P. *J. Non-Newton Fluid Mech.* **1992**, *44*, 113.